A MESH INSENSITIVE CONSTITUTIVE MODEL FOR HIGH-FIDELITY 3D SIMULATIONS OF CONCRETE STRUCTURES UNDER CYCLIC LOADING

Terry Y.P. YUEN[1], Tzu-Han WEN[2], Chung-Chan HUNG[3], and Johnson ZHANG[4]

SUMMARY

High-fidelity, three-dimensional, and nonlinear finite element analysis (NLFEA) would be inevitable to reliably analyze and design unconventional and irregular concrete structures under extreme loading. The core of NLFEM is the constitutive modeling of materials, which can be broadly classified as classical plasticity or phenomenological models. Nevertheless, many of those models could not resolve critical concrete modeling issues involving crack-induced anisotropy, change of stress transfer mechanisms under non-proportional loading, and mesh-size sensitivity. To this end, this paper presents a robust and experimentally validated constitutive model. The key features include (1) total-strain formulations and loading-history dependent internal variables, (2) cyclic stress-strain responses, (3) a novel 3D crack-plane searching algorithm, (4) multi-axial strain interaction, (5) shear-slip and re-contact of the cracks, and (6) energy-based mesh sensitivity mitigation. The proposed model was implemented into ABAQUS through the user-subroutine and applied to simulate reserved-cyclic loading tests on a shear critical column and a high-strength squat RC wall. The simulations can well capture the tested specimens' damage evolutions and load-deflection hysteresis responses. Hence, the proposed model could be a competent candidate for analyzing and designing the next generations of concrete structures with unconventional shapes.

Keywords*: mesh-insensitive; constitutive model; cracks; cyclic loading; non-proportional loading*

INTRODUCTION

The emerging 3D printed concrete techniques (Zhang et al. 2019) have raised unbounded possibilities for constructing concrete structures of unconventional and complex shapes. Since the stress and strain fields in concrete increase with the shape complexity, the unconventionally shaped concrete structures cannot be designed using the conventional methods without excessive assumptions. High-fidelity and three-dimensional nonlinear finite element analysis (NLFEA) could be the only feasible option for designing the possible next generation of concrete structures that might feature highly complicated shapes. The most important ingredient in NLFEA is undoubtedly the constitutive models of the materials.

Given the above, this paper presents a new, robust, and computationally efficient constitutive model for concrete, which is formulated based on eigendecomposition and the stress-strain behaviour on the fixed crack planes. While the Poisson effects and shear stress on the crack planes were adequately modelled in the elastic and inelastic stages, the model is applicable for non-proportional and three-dimensional loading conditions. The modelling parameters can be readily determined from or correlated with the data of standard material tests. The model was successfully implemented in ABAQUS using the user-subroutine, and its ability in capturing a wide range of realistic inelastic behaviour of concrete was demonstrated. Lastly, the model was adopted to simulate RC column

[1] *Associate Professor, National Yang Ming Chiao Tung University, email: terryyyp@nycu.edu.tw*
[2] *PhD Candidate, National Yang Ming Chiao Tung University, email: hank50403@gmail.com*
[3] *Distinguished Professor, National Cheng Kung University, email: cchung@mail.ncku.edu.tw*
[4] *Professor, Edinburgh Napier University, email: j.zhang@napier.ac.uk*

and wall tests. A good agreement between the experimental and simulated behaviour could be observed.

MODEL DEVELOPMENT

Eigen-decomposition and crack plane directions

The principal stresses σ_j or strains ε_j can be obtained by solving the eigenvalue problems for the stress tensor $\tilde{\boldsymbol{\sigma}}$ and the strain tensor $\tilde{\boldsymbol{\varepsilon}}$ in the global Cartesian coordinate.

$$\left(\tilde{\boldsymbol{\sigma}} - \sigma_j \mathbf{I}\right) \cdot \mathbf{V_j} = \mathbf{0}; \qquad \left(\tilde{\boldsymbol{\varepsilon}} - \bar{\varepsilon}_j \mathbf{I}\right) \cdot \breve{\mathbf{V}}_\mathbf{j} = \mathbf{0} \tag{1}$$

where $\mathbf{I}$ is the identity tensor; $\mathbf{V_j}$ and $\breve{\mathbf{V}}_\mathbf{j}$ are the unit direction vectors of the corresponding principal stress σ_j and principal strain $\bar{\varepsilon}_j$ respectively. The order of the principal stresses/strains is taken as $\sigma_1 \geq \sigma_2 \geq \sigma_3$. The direction vectors form the orthonormal basis i.e. $\mathbf{V_i^T} \cdot \mathbf{V_j} = \delta_{ij}$, where δ_{ij} is Kronecker delta. The inverse of the directional vectors $\mathbf{V_j}$ and $\breve{\mathbf{V}}_\mathbf{j}$ are their transposes $\mathbf{V_j^T}$ and $\breve{\mathbf{V}}_\mathbf{j}^\mathbf{T}$ respectively. By using these inverse properties and Eq. (1), we have

$$\mathbf{V_i^T} \cdot \tilde{\boldsymbol{\sigma}} \cdot \mathbf{V_j} = \boldsymbol{\sigma}; \qquad \breve{\mathbf{V}}_\mathbf{i}^\mathbf{T} \cdot \tilde{\boldsymbol{\varepsilon}} \cdot \breve{\mathbf{V}}_\mathbf{j} = \bar{\boldsymbol{\varepsilon}} \tag{2}$$

where $\boldsymbol{\sigma} = \sigma_j \delta_{ij}$ and $\bar{\boldsymbol{\varepsilon}} = \bar{\varepsilon}_j \delta_{ij}$ are the stress and total strain tensors rotated to the principal directions which have zero off-diagonal elements (i.e. shear components = 0). The above transformation is also known as contravariant tensor transformation. For isotropic elastic materials, the principal stress and principal strain directions coincide i.e. $\mathbf{V_j^T} \cdot \breve{\mathbf{V}}_\mathbf{j} = 1$. Yet, when a material deforms inelastically, the principal stress and strain directions, in general, do not coincide i.e. $\mathbf{V_j^T} \cdot \breve{\mathbf{V}}_\mathbf{j} \neq 1$. This is due to the coupling of deviatoric and volumetric strains (dilatation) during inelastic deformation, plasticity/damage induced material anisotropy, loading-history dependent plastic strain development, or the non-associated plastic flow rule. The normal directional vector of the j[th] crack plane can be directly obtained from the eigenvectors based on the assumed crack formation criteria as

$$\mathbf{V_j^c} = \mathbf{V_1} \qquad \text{if} \quad \sigma_1 = f_t > 0 \tag{3a}$$

$$\mathbf{V_j^c} = \mathbf{V_3^\perp} \qquad \text{if} \quad \sigma_3 = c_{\mathrm{ck}} \xi f_c < 0 \tag{3b}$$

where ξ is the compressive strength modification factor and its physical meaning will be introduced later.

Axial stress-strain relationship in the crack plane coordinates

Based on a series of panel shear tests, Vecchio and Collins (1986) (Vecchio and Collins 1986) and Hsu and Mansour (2005) (Mansour and Hsu 2005) developed constitutive laws for planar cracked concrete, which is represented by diagonal struts prescribed with uniaxial stress-strain relationships along ($\mathbf{V_3^c}$) and perpendicular ($\mathbf{V_1^c}$) to the crack plane as shown in *Figure 1*. To model the behaviour of such pair of diagonal struts, an improved stress-strain relationship based on Hsu and Mansour (2005) has been developed (Yuen et al. 2022) and is briefly outlined below. If the concrete along the direction $\mathbf{V_3^c}$ is under compression, then the ascending and descending branches of the compression envelope of the stress σ_3 and the equivalent axial strain ε_3 curves are expressed by Eqs. (6a) and (6b) respectively.

$$\sigma_3 = (D\zeta f_c - f_{c4}) \left[2\left(\frac{\varepsilon_3}{\zeta \varepsilon_o}\right) - \left(\frac{\varepsilon_3}{\zeta \varepsilon_o}\right)^2\right] + f_{c4} \qquad \text{if} \quad \zeta\varepsilon_o \leq \varepsilon_3 \leq 0 \tag{4a}$$

$$\sigma_3 = \max\left(D\zeta f_c \left[1 - \left(\frac{\varepsilon_3/(\zeta\varepsilon_o) - 1}{a_c/\zeta - 1}\right)^2\right], c_{min}\, \zeta f_c\right) \qquad \text{if} \quad \zeta\varepsilon_o > \varepsilon_3 \tag{4b}$$

The state-variables D and ζ, which control the softening of the compressive strength $f_c < 0.0$, are calculated by Eq. (7) and Eq. (8) respectively; f_{c4} is defined in *Figure 1*; D depends on the maximum compressive strain $\varepsilon_c^{\mathrm{Max}}$ in the past loading history, while ζ is the multiplication of three strength reduction factors $\zeta_1(f_c)$, and $\zeta_2(\varepsilon_1 \geq 0)$; a_c is a constant governing the decay rate of the compressive stress after the peak and its value depends on the mesh size (Yuen et al. 2022). The second term of Eq. (4b) represents the minimum compressive strength and is used to prevent numerical instability. The factor c_{min} is set as 0.01 in this study.

If the concrete along the direction $\mathbf{V_1^c}$ is under tension, then the stress-strain envelope can be expressed by Eqs. (5a) and (5b) for the pre-peak and post-peak branches respectively.

$$\sigma_1 = E_c \varepsilon_1 \qquad \text{if} \quad \varepsilon_r \geq \varepsilon_1 \geq 0 \tag{5a}$$

$$\sigma_1 = \alpha_{CD} f_r \left(\frac{\varepsilon_r}{\varepsilon_1}\right)^{a_t} \qquad \text{if} \quad \varepsilon_1 > \varepsilon_r \tag{5b}$$

where f_r is the peak tensile stress and $\varepsilon_r = f_r/E_c$ is the corresponding tensile strain; a_t is a mesh-size

dependent constant governing the decay rate of the tensile stress after the peak; α_{CD} is the ratio between the residual compressive strength f_{c2} (*Figure 1*) and the peak compressive strength $\zeta_1 f_c$ as defined by Eq. (6).

$$\alpha_{CD} = f_{c2}/(\zeta_1 f_c) \leq 1.0 \quad (6)$$

Hence, the tensile strength diminishes with the concrete crushing as being quantified by the compressive strength degradation. It is noted that the axial loading directions of the struts on $\mathbf{V}_1^c$ & $\mathbf{V}_3^c$ can be completely reversed during the cyclic loading. The modelled cyclic behaviour is shown in **Figure 1**.

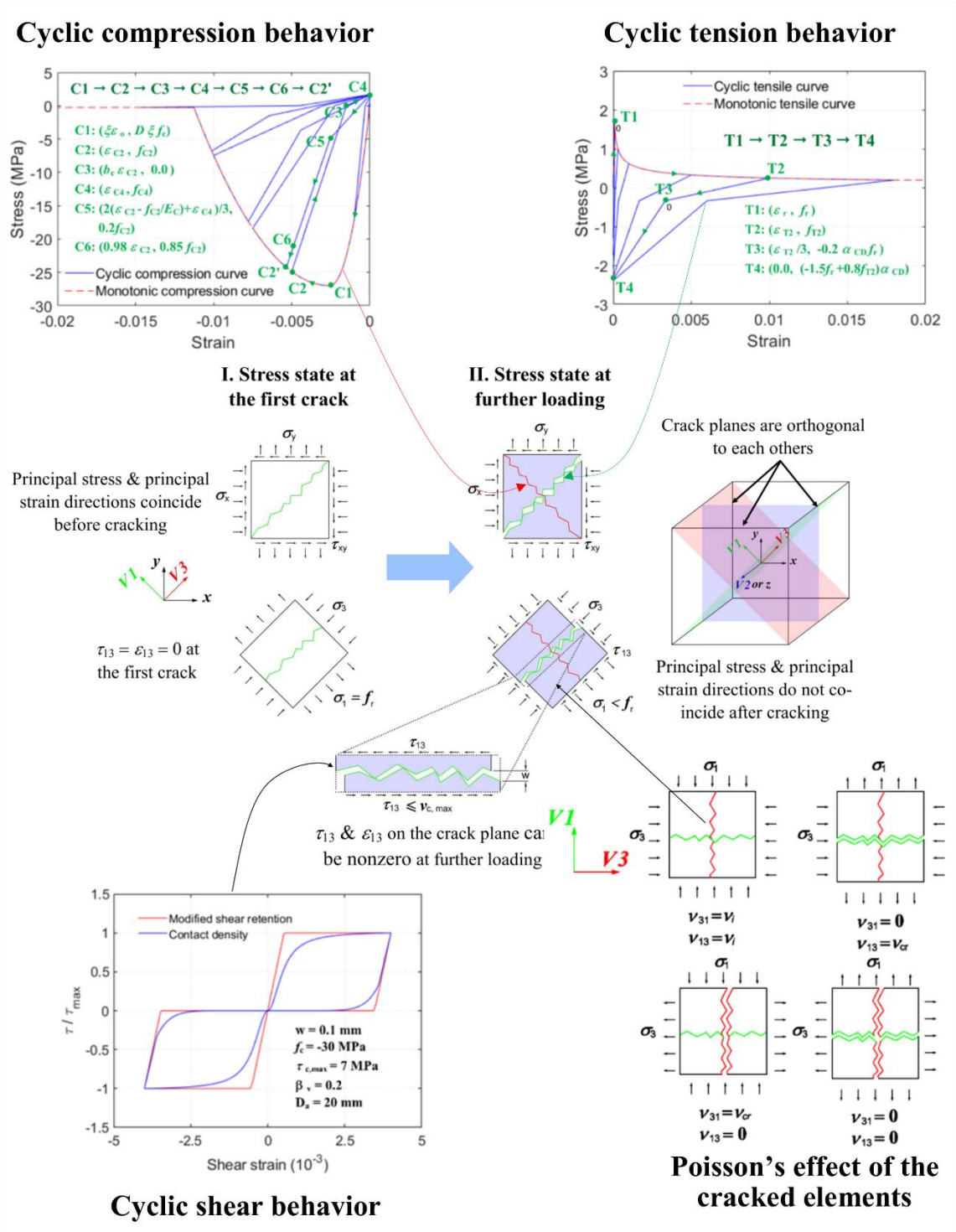

Figure 1. Stress states at the first crack and further loading (Yuen et al. 2022).

Shear behaviour

At the crack initiation, the shear stress on the crack plane is zero but the shear stiffness will not vanish due to the aggregate interlocking. Therefore, shear stress will be present on crack planes if the shear strain is induced during the subsequent loading (Maekawa et al. 2003). The maximum shear stress τ'_{cij} on a crack plane $\mathbf{V_i^c}$ subjecting to shear in $\mathbf{V_j}$ is calculated by Eq. (7), which is based on the aggregate interlocking analysis by Walraven (Walraven 1981).

$$\tau'_{cij} \le \tau_{ci,MCFT} = \hat{\tau}_{ci} + 1.64\langle -\sigma_i \rangle - 0.148\frac{\langle -\sigma_i \rangle^2}{\hat{v}_{ci}} \tag{7}$$

where $\langle -\sigma_i \rangle = \sigma_i$ if $\sigma_i < 0$ or $\langle -\sigma_i \rangle = 0$ if $\sigma_i \ge 0$ and hence the last two terms of Eq. (7) account for the pressure-dependent friction. The maximum shear stress $\tau_{ci,MCFT}$ under the absence of normal compression on the crack plane $\mathbf{V_i^c}$ is given by Eq. (14).

$$\hat{\tau}_{ci} = \frac{0.18\sqrt{-f_c}}{0.31+24w_{i,max}/(D_a+16)} \qquad \text{(in mm, N)} \tag{8}$$

The maximum shear stress $\hat{v}_{ci}$ is a function of the maximum aggregate size D_a and the maximum crack width $w_{i,amx}$. In smeared crack models, w_i can be estimated from the crack strain $\varepsilon_i^{cr} = \varepsilon_i - f_r/E_c \ge 0$ and the element characteristic length crack l_e as

$$w_{1,max} = \varepsilon_{1,max}^{cr}\, l_e \tag{9}$$

The shear stiffness of cracked concrete can be independent of Young's modulus and the Poisson's ratio and a reduced shear modulus can be assumed. Furthermore, the maximum shear stress in Eq. (7) decreases with the crack opening w only. But as the inelastic strain develops under compression, the shear strength would also degrade along with the compressive strength. The most common way to model this effect is to use a damage state-dependent shear retention factor $\beta_v \le 1$ (Chung and Ahmad 1995; Hung et al. 2013) to reduce the effective shear stiffness, i.e. $G_{eq} = \beta_v G_c$, where $G_c = E_c/\big(2(1+\nu_c)\big)$ is the initial shear modulus. Hence,

$$\tau_{ij}^c = 2\beta_v G_c \varepsilon_{ij} \le \tau'_{cij} \tag{10}$$

The shear stress on the crack plane as modelled by Eq. (18), which is adopted in this study, will have a more gradual change across different damage states. Meanwhile, the imperfect contact of the crack surfaces would lead to nonlinear elastic shear stress-strain behaviour. If modelling of this behaviour is needed, more complicated shear models such as the contact density model (Maekawa et al. 2003) can be adopted. Based on the above model, the maximum attainable shear stress across a crack would degrade with the normal crack opening w but increase with the aggregate size D_a, which is an important feature of shear stress transfer due to aggregate interlocking (Walraven 1981). The relations among the maximum attainable shear stress, the crack width, and aggregate size are illustrated in **Figure 1**.

Poisson's effect

In displacement-based numerical analysis, the deformation gradient or stain increments are given at each element integration point at a time step. The total normal strain increment $\delta\bar{\varepsilon}_{ii}$ $(i = 1,2,3)$ of an element cannot be directly used to calculate the uniaxial stresses but the strain increment due to Poisson's effect shall be eliminated to obtain the equivalent uniaxial strain increments $\delta\varepsilon_{ii}$ (Hung and Li 2013) as

$$\delta\bar{\varepsilon}_{ij} = \delta\varepsilon_{ij} - \textstyle\sum_{m=1}^{3}\nu_{im}\delta\varepsilon_{mj}\big(1-\delta_{mj}\big) \qquad (i=j) \tag{11a}$$

$$\delta\bar{\varepsilon}_{ij} = \delta\varepsilon_{ij} \qquad (i\ne j) \tag{11b}$$

The transformation can be expressed in a matrix form as

$$\begin{bmatrix}\delta\varepsilon_{11}\\ \delta\varepsilon_{22}\\ \delta\varepsilon_{33}\\ \delta\varepsilon_{12}\\ \delta\varepsilon_{23}\\ \delta\varepsilon_{31}\end{bmatrix} = \frac{1}{|\mathcal{L}|}\begin{bmatrix} 1-\nu_{32}\nu_{23} & \nu_{12}+\nu_{13}\nu_{32} & \nu_{13}+\nu_{12}\nu_{23} & & & \\ \nu_{21}+\nu_{31}\nu_{23} & 1-\nu_{13}\nu_{31} & \nu_{23}+\nu_{21}\nu_{13} & & \mathbf{0} & \\ \nu_{31}+\nu_{21}\nu_{32} & \nu_{32}+\nu_{12}\nu_{31} & 1-\nu_{12}\nu_{21} & & & \\ & & & |\mathcal{L}| & 0 & 0 \\ & \mathbf{0} & & 0 & |\mathcal{L}| & 0 \\ & & & 0 & 0 & |\mathcal{L}| \end{bmatrix}\begin{bmatrix}\delta\bar{\varepsilon}_{11}\\ \delta\bar{\varepsilon}_{22}\\ \delta\bar{\varepsilon}_{33}\\ \delta\bar{\varepsilon}_{12}\\ \delta\bar{\varepsilon}_{23}\\ \delta\bar{\varepsilon}_{31}\end{bmatrix} \tag{12}$$

where $|\mathcal{L}| = 1-\nu_{32}\nu_{23}-\nu_{12}\nu_{21}-\nu_{13}\nu_{31}-\nu_{12}\nu_{23}\nu_{31}-\nu_{21}\nu_{32}\nu_{13}$.

The Poisson' ratio of uncracked concrete is isotropic $\nu_{ij} = \nu_c$ and is a constant of 0.2. The cracked concrete becomes an anisotropic material and, if the crack is opening in $\mathbf{V_i^c}$ that $\delta\varepsilon_i > 0$, the effective Poisson' effect can be represented by the following empirical relations which are based on the Hsu/Zhu ratio (Hsu and Zhu 2002; Mansour and Hsu 2005):

$$\nu_{ij} = \nu_{\mathrm{cr}} = \min\big[0.2 + 850\max(|\varepsilon_{sl}|,|\varepsilon_{st}|), \nu_{\mathrm{cr,max}}\big]\, u\big(\sigma_{T3,j} - \sigma_{\mathrm{j}}\big) \tag{13a}$$

$$\nu_{ji} = 0.0 \tag{13b}$$

Hence, the crack opening/strain in $\mathbf{V_i^c}$ will not induce lateral strains in $\mathbf{V_j^c}$ due to the Poisson' effect, meanwhile

the axial strain in $\mathbf{V}_j^c$ (if uncracked) will incur higher lateral strains in $\mathbf{V}_i^c$ with $\nu_{ij} > 0.2$ up to $\nu_{\mathrm{cr,max}}$. If the crack in $\mathbf{V}_i^c$ is closed in the next loading half-cycle, then one of the following situations applies: (i) if $\mathbf{V}_j^c$ is uncracked or the crack is closed, then $\nu_{ji}\, and\, \nu_{ij} = 0.2$; (ii) if the crack in $\mathbf{V}_j^c$ is opening, then ν_{ji} is calculated by Eq. (13) (with indexes *i* and *j* swapped) and $\nu_{ij} = 0$. The unit step function $u(\sigma_{T3,j} - \sigma_j) = 1$ if $\sigma_{T3,j} - \sigma_j > 0$ else $u(\sigma_{T3,j} - \sigma_j) = 0$ is added to the original relation of the Hsu/Zhu ratio to account for the effect of crack opening/closure under cyclic loading. $\sigma_{T3,j}$ is the stress on the crack plane *j* at the stiffness unilateral point T3 ($\varepsilon_{T2}/3,\ -0.2\alpha_{CD} f_r$) defined in *Figure 1*. Therefore, the recovery of the Poisson's ratio will conform to the complete crack closure from tension to compression. If the crack was also formed in $\mathbf{V}_j$ in the previous loading cycle but has not been closed completely in the current loading cycle, then no lateral strain would be induced due to the Poisson' effect, i.e. $\nu_{ij} = 0.0$ in Eq. (12). Furthermore, it can be readily shown that the transformation of Eq. (11) with Eq. (12) will lead to a non-symmetric stiffness matrix. As discussed above, this is the property of inelastic materials with non-associated plastic flow rules, which can be reflected in the above relations. And the principal stress and principal strain directions of a material deforming inelastically with a non-symmetric stiffness matrix would certainly be noncoincident.

Mitigating mesh-sensitivity and mesh size restrictions

It is well recognised that mesh sensitivity in continuum finite element analysis would be resulted from the softening stress-strain curves due to the localised inelastic deformation (Krätzig and Pölling 2004; Liu et al. 2020; Nguyen et al. 2018) that can significantly affect the simulated post-peak structural responses. To reduce the mesh sensitivity, the descending branches of the stress-strain curves (4b) and (5b) shall be dependent on the mesh size or the element characteristic length (ABAQUS Inc. 2020). A convenient method to mitigate the mesh-sensitivity is by using the tested stress-displacement curves and the equivalent strain can be obtained by dividing the displacement δ with the element characteristic length l_e, over which the inelastic deformation in the actual damage or fracture process zone is smeared. Another method is to adjust the decay rate of the descending branches based on the element characteristic length (Krätzig and Pölling 2004; Liu et al. 2020) or the width of the crack/damage band (Bažant and Oh 1983) such that the localised energy dissipation of every element is consistent. In this study, the latter method is adopted for adjusting the softening stress-strain curves. Integrating Eqs. (4b) and (5b) with respect to the post-peak displacement with $\delta = \varepsilon l_e$ and excluding the strength modification factors, we have

$$\Theta_t = \int_{\delta_r(\sigma_t=f_r)}^{\infty(\sigma_t=0)} f_r \left(\frac{\delta_r}{\delta_1}\right)^{a_t} d\delta_1 = \frac{f_r^2 l_e}{E(a_t-1)} \tag{14}$$

$$\Theta_c = \int_{\delta_o(\sigma_c=f_c)}^{\delta_u(\sigma_c=0)} f_c \left[1 - \left(\frac{\delta_3/\delta_o - 1}{a_c - 1}\right)^2\right] d\delta_3 = \frac{2}{3} f_c \delta_o (a_c - 1) \tag{36}$$

For the evaluation of Eq. (14), the relationship $\delta_u = a_c \delta_o$ when $\sigma_c = 0$ was used. As $\varepsilon_1 l_e$ can be regarded as the crack opening displacement, Θ_t is equivalent to the mode I fracture energy G_t (Bažant and Oh 1983). From Eq. (14), a_t can be directly evaluated as

$$a_t = 1 + \frac{f_r^2 l_e}{E G_t} = 1 + \frac{l_e}{l_{ft}} \tag{15}$$

in which $l_{ft} = E G_t / f_r^2$ is commonly known as the characteristic length of fracture (Rosselló et al. 2006). If the element size is too large, the snap-back phenomenon along with the material softening may occur (Bažant and Oh 1983; Krätzig and Pölling 2004). Following (Krätzig and Pölling 2004; Nakamura and Takeshi 2000), the localised crushing energy G_c relevant to the softening branch is estimated as:

$$G_c \approx \Theta_c + \frac{1}{2} f_c \delta_o (1 - b_c) = \frac{2}{3} f_c \delta_o (a_c - 1) + \frac{1}{2} f_c \delta_o (1 - b_c) \tag{16}$$

To ensure the consistency of the localised crushing energy by the elements, the following condition is enforced using Eq. (36) and $\delta_o = \varepsilon_o l_e$

$$G_c = \frac{f_c \varepsilon_o l_e}{3} \left[2a_c - \frac{3b_c + 1}{2}\right] \tag{17}$$

Rearranging Eq. (17) for a_c, we have

$$a_c = \frac{3G_c}{2 f_c \varepsilon_o l_e} + \frac{3b_c + 1}{4} \tag{18}$$

Similarly, the element length is restricted as below to prevent snap-back behaviour under compression:

$$l_e \le l_{fc} = \frac{G_c}{f_c \varepsilon_o} \tag{19}$$

Uniaxial compressive stress-strain behaviour of concrete is often determined from compressive tests on the cylindrical specimen. But the length of the compressive fracture process zone l_{cp} would not spread over the whole specimen and it can be estimated using the following equation (Nakamura and Takeshi 2000)

$$l_{cp} = \frac{1300}{\sqrt{f_c}} \quad \text{(in mm, MPa)} \tag{20}$$

For instance, the localised crushing energy of grade C30 concrete with $\varepsilon_o = 0.0023$, and $f_c = 30$MPa (CEB-FIP 2012) can be calculated by Eq. (20) with $l_e = l_{cp} = 237$ mm and Eq. (17) that gives $G_c = 46.6$ N/mm. The element size shall be limited as follows

$$\min(l_{ft},\ l_{fc}) > l_e \tag{21}$$

SIMULATION OF A FULL-SCALE SHEAR-CRITICAL RC COLUMN TEST

To investigate the performance of the proposed model in simulating the seismic behaviour of concrete structures, a cyclic loading test (Huy et al. 2022) on a full-scale shear-critical RC column of dimensions = $0.8 \times 0.8 \times 3.2$ m was simulated. The test was performed using the Multi-Axial Testing System (MATS) at the National Centre for Earthquake Engineering Research (NCEER, ROC). The test setup, column dimensions, reinforcement detailing, loading protocol are shown in **Figure 2**. The transverse reinforcement was not sufficiently provided in this column and therefore, it failed in shear before yielding of the longitudinal reinforcement could occur. The column was subject to a constant axial load of 2560 kN and varying displacement-controlled horizontal loading. Three-dimensional finite element models, which faithfully reproduce the specimen geometries, were developed using ABAQUS with the material user-subroutine (ABAQUS Inc. 2020; Yuen et al. 2022) mentioned above. The reinforcing bars were modelled with 2-node linear 3D beam elements, while the concrete was modelled with 8-node linear 3D brick elements. Elastic perfectly plastic stress-strain relationships were applied on the rebar elements. The Young's modulus was 200 GPa and the tested yield strengths were 473 MPa and 400 MPa for ϕ32(#10) longitudinal rebar and ϕ6(#2) transverse rebar respectively. The compressive strength of concrete was 43MPa. The mesh sensitivity was also investigated, and the tested mesh sizes of both concrete and rebar elements were 150 mm, 100 mm, and 50 mm. The mesh size-independent and dependent model parameters are summarised in **Table 1**.

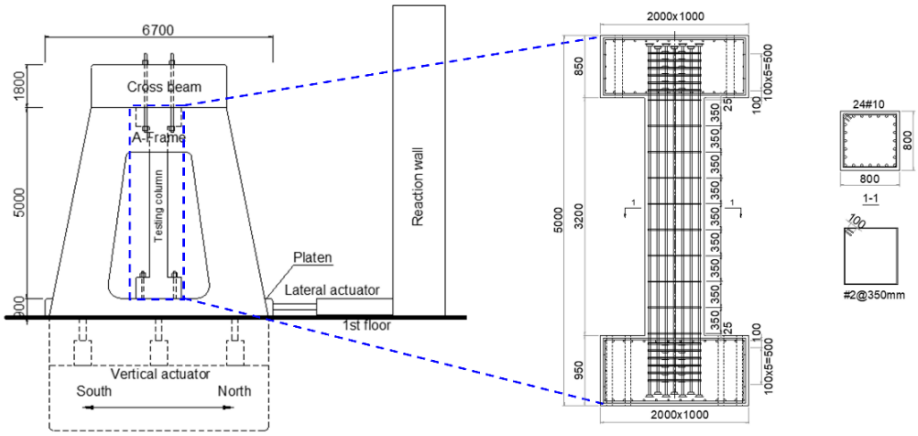

Figure 2. Full-scale shear-critical RC column test (Huy et al. 2022; Yuen et al. 2022): (a) test set-up; (b) rebar details (dimensions in mm).

Table 1. Concrete model parameters for the RC column and wall simulations.

Model parameters	RC column with 150 mm mesh	RC column with 100 mm mesh	RC column with 50 mm mesh	RC wall with 50 mm mesh
E_c (GPa)	22.71	22.71	22.71	32.29
ν_c	0.2	0.2	0.2	0.2
f_c (MPa)	-41	-41	-41	-73.7
f_r (MPa)	3.57	3.57	3.57	4.3
b_C	0.5	0.5	0.5	0.5
ψ	0	0	0	0
D_a (mm)	20	20	20	20
β_v	0.2	0.2	0.2	0.2
μ	0.7	0.7	0.7	0.6
$\nu_{cr,max}$	1.0	1.0	1.0	1.0
l_e (mm)	150	100	50	50
a_c	5.19	7.48	14.33	17.51
a_t	1.59	1.39	1.20	1.11

The hysteresis loops, the evolution of the crack patterns of the column during the cyclic loading test and the simulated results are shown in **Figure 3.** Inclined interacting flexural-shear cracks were observed in the test at around 0.75% drift, leading to reduced lateral stiffness. Eventually, a large diagonal shear crack occurred when the column was loaded beyond 0.75% to 1.0% drift, where the peak strength was reached and significant strength degradation occurred afterwards. The proposed model can capture the degradation and shear slip and re-contact behaviour well. Furthermore, similar hysteretic behaviour can be obtained in all models with 50 mm, 100 mm, and 150 mm mesh, the sensitivity of the simulations with the proposed model to the mesh size is low.

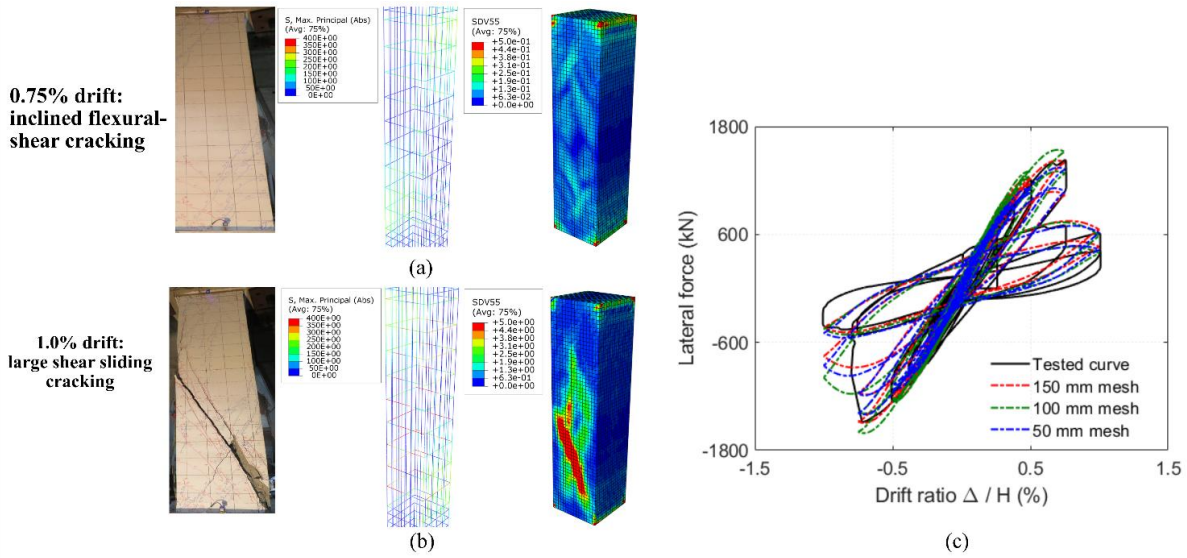

Figure 3. Comparison of tested and simulated column behaviour (Huy et al. 2022; Yuen et al. 2022): (a) at 0.75% drift; (b) at 1.0% drift; (c) hysteresis loops.

SIMULATION OF SHEAR-CRITICAL RC WALL TEST

Another case study is the simulation of a high-strength RC squat wall with an aspect ratio of 0.5 (specimen code: HHH-0.5), which was tested at the National Taiwan University of Science and Technology (Cheng et al. 2021). Besides the web reinforcement, confinement reinforcement was provided along the boundary zones and dowel reinforcement was provided at the wall base, as shown in **Figure 4**. The rebar size and yield strength for the vertical, web, and dowel reinforcement were ϕ13 (#4, diameter = 12.7 mm), while the confinement reinforcement was composed of ϕ10 (#3, = 9.53 mm) closed-hoops of 864 MPa. The tested concrete strength of the wall specimen was 73.7 MPa. The wall was reverse-cyclically loaded in the lateral direction along the centreline of the top-loading beam. Similarly, a FE model was developed for the wall specimen using the proposed constitutive model and the modelling approach described above. Despite the mitigated mesh sensitivity of the proposed model demonstrated in the above column simulation, the mesh size is set as 50 mm to depict the detailed damage patterns. The concrete model parameters are provided in **Table 1**.

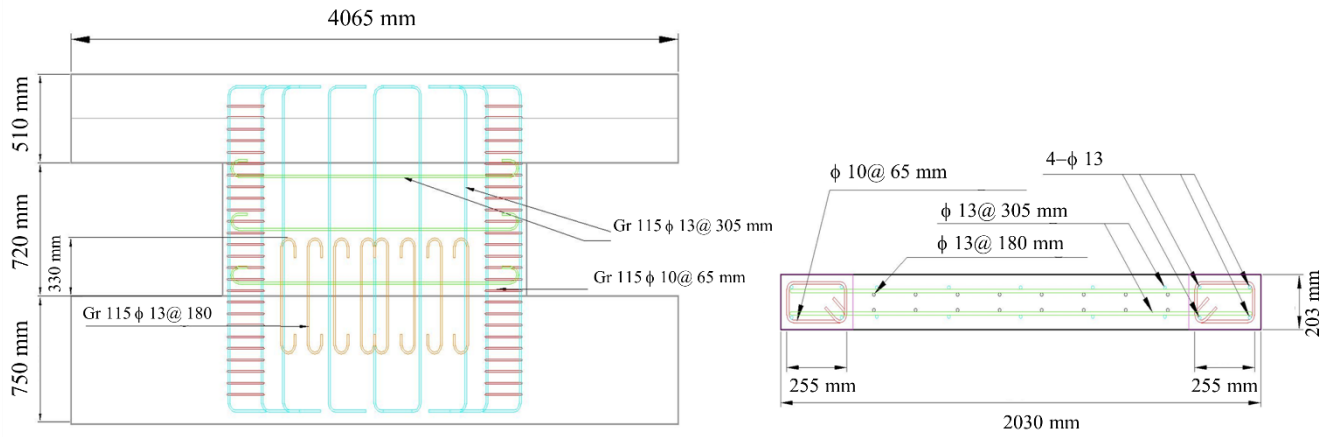

Figure 4. Reinforcement details of the high strength squat shear wall (Cheng et al. 2021).

Figure 5 shows the comparisons of the tested (Cheng et al. 2021) and simulated damage patterns (Wen et al. 2022) and the hysteresis behaviour. The web region of the wall mainly suffered diagonal cracking before 0.75% drift. Meanwhile, the confinement reinforcement could effectively restraint the diagonal shear crack formation and propagation that the cracks in the confined zones were dominantly propagating horizontally. In the late loading stage, a large horizontal shear sliding crack was formed right above the dowel reinforcement. After that, significant strength and stiffness degradation can be observed in the hysteresis loops. It shows that the dowel reinforcement can effectively prevent the base sliding failure. The simulation with the proposed model can well capture these observed behaviours. Furthermore, the simulated hysteresis also agrees well with the tested results.

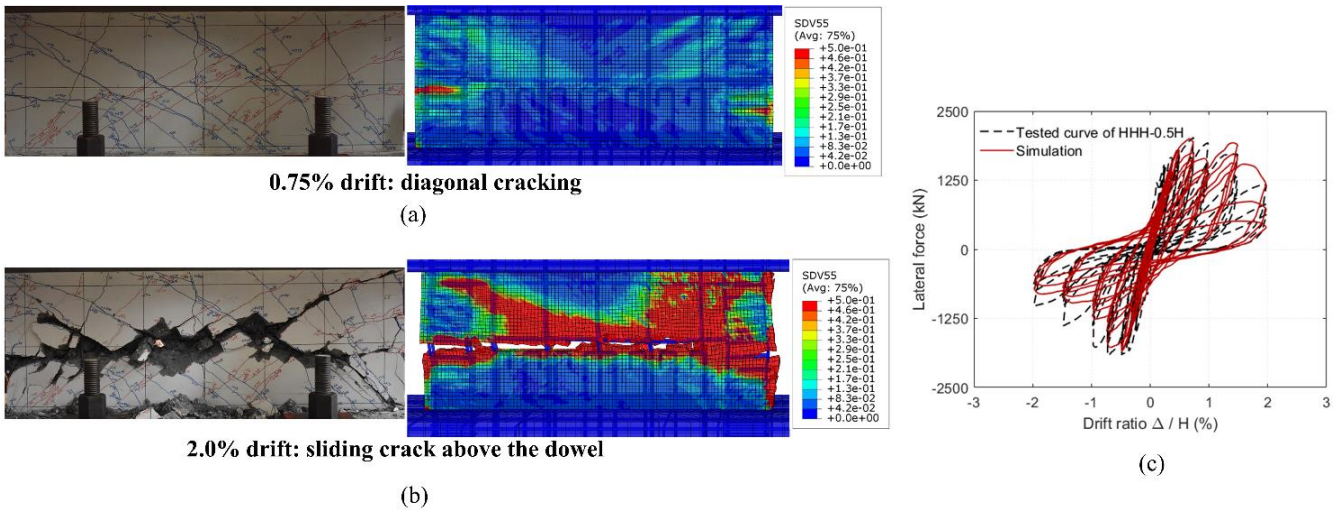

Figure 5. Comparison of tested (Cheng et al. 2021) and simulated wall behavior (Wen et al. 2022): (a) at 0.75% drift; (b) at 2.0% drift; (c) hysteresis loops.

CONCLUSIONS

Rigorous nonlinear load-response analysis would be indispensable for the analysis and design of non-conventional and irregular concrete structures. The core of nonlinear response analysis is the constitutive modelling of materials. This paper presents a recently developed concrete constitutive model that can tackle a number of issues of the existing models. The model was successfully applied to simulate the reversed-cyclic load-response behaviour of a shear-critical RC column and a high-strength RC squat wall. Based on the analysis results, the following conclusions are drawn.

1. The proposed model employs the eigendecomposition method and prescribed crack formation criteria to determine the crack plane coordinate. The crack planes are assumed to be mutually orthogonal to each other.

2. The axial cyclic stress-strain responses of the crack planes and their interactions are modelled through the equivalent uniaxial strain transformation using the modified Hsu/ Zhu ratios. Meanwhile, a modified shear retention model with cyclic behaviour resembling the contact density theory is adopted to model the cyclic shear stress-strain behaviour of the crack planes.

3. A regularisation method for the model parameters depending on the mesh size was developed to mitigate the mesh-sensitivity problem in finite element implementation due to the material softening.

4. The model was implemented in ABAQUS using the subroutine for user materials. Reversed-cyclic loading tests on a full-scale shear-critical column and a squat RC wall were simulated for the model validation.

5. The simulations can comprehensively capture the damage patterns and propagation of the tested RC column and the RC wall from the early to the late loading stages. The simulated load-deflection hysteresis responses also well agree with the test results.

ACKNOWLEDGEMENT

The authors would like to express their gratitude for the funding support by the Ministry of Science and Technology

(MOST), R.O.C. under Grand Numbers 110-2221-E-A49 -133 -, 109-2636-E-006-015, 109-2636-E-009 -015-., and Royal Academy of Engineering-Industrial Fellowship (IF\192023). We sincerely thank Prof. Min-Yuan Cheng and Dr. Marnie Giduquio from the Dept. of Civil and Construction Engineering, National Taiwan University of Science and Technology for providing the experimental data on high-strength squat RC walls.

REFERENCES

ABAQUS Inc. (2020), "Abaqus/Explicit User Subroutines: VUMAT," *Abaqus User Subroutines Reference Guide*.

Bažant, Z. P., and Oh, B. H. (1983). "Crack band theory for fracture of concrete." *Matériaux et Constructions*, Vol. 16, No. 3, 155–177.

CEB-FIP. (2012), *Model Code 2010 - Final version, Vol. 1. fib Bulletin 65.Federation Internationale du Beton, Lausanne.*, fédération internationale du béton, Bulletin 66, Lausanne, Switzerland.

Cheng, M.-Y., Wibowo, L. S. B., Giduquio, M. B., and Lequesne, R. D. (2021), "Strength and deformation of reinforced concrete squat walls with high-strength materials," *ACI Structural Journal*, Vol. 118, No. 1, 125–137.

Chung, W., and Ahmad, S. H. (1995), "Analytical model for shear critical reinforced-concrete members," *Journal of Structural Engineering*, Vol. 121, No. 6, 1023–1029.

Hsu, T. T., and Zhu, R. H. (2002), "Softened membrane model for reinforced concrete elements in shear," *ACI Structural Journal*, Vol. 99, No. 4, 460–469.

Hung, C.-C., and Li, S.-H. (2013), "Three-dimensional model for analysis of high performance fiber reinforced cement-based composites," *Composites Part B: Engineering*, Vol. 45, No. 1, 1441–1447.

Hung, C.-C., Su, Y.-F., and Yu, K.-H. (2013), "Modeling the shear hysteretic response for high performance fiber reinforced cementitious composites," *Construction and Building Materials*, Vol. 41, 37–48.

Huy, P. P. A., Yuen, T. Y., Hung, C.-C., and Mosalam, K. M. (2022), "Seismic behaviour of full-scale lightly reinforced concrete columns under high axial loads," *Journal of Building Engineering*, Vol. 56, 104817.

Krätzig, W. B., and Pölling, R. (2004), "An elasto-plastic damage model for reinforced concrete with minimum number of material parameters," *Computers and Structures*, Vol. 82, No. 15–16, 1201–1215.

Liu, C., Yang, Y., Wang, J.-J., Fan, J.-S., Tao, M.-X., and Mo, Y. L. (2020), "Biaxial reinforced concrete constitutive models for implicit and explicit solvers with reduced mesh sensitivity," *Engineering Structures*, Vol. 219, 110880.

Maekawa, K., Okamura, H., and Pimanmas, A. (2003), *Non-Linear Mechanics of Reinforced Concrete*. CRC Press.

Mansour, M., and Hsu, T. T. C. (2005). "Behavior of reinforced concrete elements under cyclic shear. II: theoretical model," *Journal of Structural Engineering*, Vol. 131, No. 1, 54–65.

Nakamura, H., and Takeshi, H. (2000), "Compressive fracture energy and fracture zone length of concrete," *US-Japan Seminar on Post-Peak Behavior of Reinforced Concrete Structures Subjected to Seismic Loads: Recent Advances and Challenges on Analysis and Design*, Tokyo, Japan, 471–487.

Nguyen, T. H. A., Bui, T. Q., and Hirose, S. (2018), "Smoothing gradient damage model with evolving anisotropic nonlocal interactions tailored to low-order finite elements," *Computer Methods in Applied Mechanics and Engineering*, Vol. 328, 498–541.

Rosselló, C., Elices, M., and Guinea, G. V. (2006), "Fracture of model concrete: 2. Fracture energy and characteristic length," *Cement and Concrete Research*, Vol. 36, No. 7, 1345–1353.

Vecchio, F. J., and Collins, M. P. (1986), "The modified compression-field theory for reinforced concrete elements

subjected to shear," *ACI JOURNAL*, Vol. 19, No. 16, 219–223.

Walraven, J. C. (1981), "Fundamental analysis of aggregate interlock," *Journal of the Structural Division, ASCE*, Vol. 107, No. ST11, 2245–2270.

Wen, T.-H., Hung, C.-C., Zhang, H., Huy, P., and Yuen, T. (2022), "High-fidelity nonlinear cyclic response simulations of squat RC shear walls," *Structural Engineering*, Vol. 37, No. 2, 99-112 (in Chinese).

Yuen, T. Y. P., Wen, T.-H., Hung, C.-C., Zhang, H., Pham, P. A. H., and Deng, Y. (2022), "An eigendecomposition-based and mesh-sensitivity reduced constitutive model for nonlinear analysis of concrete structures under non-proportional cyclic loading," *Journal of Building Engineering*, Vol. 47, 103875.

Zhang, J., Wang, J., Dong, S., Yu, X., and Han, B. (2019), "A review of the current progress and application of 3D printed concrete," *Composites Part A: Applied Science and Manufacturing*, Vol. 125, 105533.